Applied Catalysis B: Environmental 147 (2014) 546–553

Contents lists available at ScienceDirect

Applied Catalysis B: Environmental

journal homepage: www.elsevier.com/locate/apcatb

Novel visible light induced Co_3O_4-g-C_3N_4 heterojunction photocatalysts for efficient degradation of methyl orange

Changcun Han[a,b], Lei Ge[a,b,*], Changfeng Chen[b], Yujing Li[b], Xinlai Xiao[b], Yuanna Zhang[b], Lele Guo[b]

[a] Key Laboratory of Heavy Oil Processing, College of Science, China University of Petroleum Beijing, No. 18 Fuxue Rd. , Beijing 102249, People's Republic of China
[b] Department of Materials Science and Engineering, College of Science, China University of Petroleum Beijing, No. 18 Fuxue Rd. , Beijing 102249, People's Republic of China

ARTICLE INFO

Article history:
Received 2 July 2013
Received in revised form
10 September 2013
Accepted 22 September 2013
Available online 29 September 2013

Keywords:
Graphitic carbon nitride
Cobalt oxides
Photocatalysis
Heterojunction photocatalysts

ABSTRACT

Novel visible-light-induced Co_3O_4-g-C_3N_4 heterojunction photocatalysts were synthesized via a facile mixing-and-heating method. The as-prepared samples were characterized by X-ray diffraction (XRD), scanning electron microscopy (SEM), transmission electron microscopy (TEM), high-resolution transmission electron microscopy (HRTEM), ultraviolet–visible diffuse reflection spectroscopy (DRS), electron spin resonance (ESR) and photoluminescence spectroscopy (PL). The heterojunction photocatalysts exhibit a significantly enhanced photocatalytic activity in degrading methyl orange (MO). The optimal Co_3O_4 content with the highest photocatalytic activity was determined to be 0.2 wt%. The synergetic effect between Co_3O_4 and g-C_3N_4 plays an important role in promoting photo-generated carrier separation. The ESR and PL results reveals that the enhanced photocatalytic activity of Co_3O_4-g-C_3N_4 was mainly due to the superior amount and longer lifetime of oxidative radicals ($^{\bullet}O_2^-$), as well as the efficient separation of charge carriers. Possible mechanism is proposed for the high photocatalytic activity of heterojunction structures, to guide the design of photocatalysts.

1. Introduction

The demand for clean energy technology has attracted research on using semiconductors as photocatalysts for water splitting and pollutants degradation [1–4]. Among various semiconductor photocatalysts, TiO_2 is considered as one of the most promising photocatalysts [5,6]. However, TiO_2 could only respond to photons with wavelength in UV range which takes only about 4% of solar energy and thus limits its application to a great extent [7–10]. Therefore, the creation of simple, efficient, and sustainable photocatalysts that work well with visible light is a major challenge in this field. Recently, various multicomponent oxides [11], sulfides [12,13], oxynitrides [14], such as $BiVO_4$ [15–17], CdS [18], Bi_2WO_6 [19], g-C_3N_4 [20,21], WO_3 [22], $SrTiO_3$ [23], etc. have been developed for organic pollutants degradation or water splitting. However, the rapid recombination rate and long migration distance of the photo-generated charge carriers influence the photocatalytic efficiency. Therefore, designing and exploring photocatalysts with higher efficiency has attracted intensive efforts in the field of photocatalysis.

Recently, Wang et al. [24] reported that the polymeric graphitic carbon nitride (g-C_3N_4) shows superior H_2 or O_2 evolution activities via water splitting under visible light irradiation in presence of sacrificial donor or acceptor. The g-C_3N_4 has several allotropes with diverse properties among which the graphitic phase is more stable under ambient conditions. It has attracted considerable attention as a promising "metal-free" photocatalyst within visible-light region, with ease of synthesis and good chemical stability [25]. Nevertheless, low separation efficiency of photogenerated electron–hole pairs is a main issue limiting the application of g-C_3N_4. Numerous attempts have been made to improve its photocatalytic performance. Yan et al. [26] synthesized mesporous g-C_3N_4 and used it as a photocatalyst to degrade organic dyes under visible light irradiation. Recently, the novel TaON-g-C_3N_4 [27] and TiO_2-g-C_3N_4 [28] composite photocatalysts were prepared and used for the photodegradation of rhodamine B as well as water splitting. Our group has reported Ag/g-C_3N_4 [29], Bi_2WO_6-g-C_3N_4 [30], MWNTS-g-C_3N_4 [31], and PANI-g-C_3N_4 [32] composite photocatalysts, and demonstrated that the modified g-C_3N_4 exhibited enhanced visible light photocatalytic activities for H_2 evolution or organic dyes degradation.

* Corresponding author. Tel.: +86 10 89739096.
E-mail address: gelei08@163.com (L. Ge).

0926-3373/$ – see front matter © 2013 Elsevier B.V. All rights reserved.
http://dx.doi.org/10.1016/j.apcatb.2013.09.038

Cobalt oxide (Co_3O_4) has intrigued intensive interest as a p-type semiconductor due to its interesting electronic and magnetic properties [33–36]. Co_3O_4 can be used as catalyst for low-temperature oxidation of CO [37], or in high performance supercapacitors [38], and it is regarded as the most versatile oxide material among transition metal oxides. Recently, it has been reported that the Co_3O_4/$BiVO_4$ [36] composite showed superior activity in phenol degradation under visible light irradiation, which can be explained by the formation of p–n heterojunction semiconductor structure. Very recently, Wang et al. [39] loaded Co_3O_4 as water oxidation catalysts (WOC) on the g-C_3N_4 photocatalysts, and investigated the photocatalytic evolution of oxygen from water. However, the photocatalytic degradation of organics and the mechanism for the Co_3O_4-g-C_3N_4 composites material is not clear. Our group also synthesized cobalt–phosphate (Co–Pi) modified g-C_3N_4 with high water splitting activity [7], proving that the cobalt-based species can be applied to enhance the photocatalytic performance in the C_3N_4 based materials.

In this study, considering the synergetic effect between Co_3O_4 and polymeric g-C_3N_4, the Co_3O_4-g-C_3N_4 heterojunction photocatalysts were synthesized to degrade the organics dyes for the first time. The photocatalytic activity of g-C_3N_4 can be significantly enhanced with the addition of Co_3O_4 species under visible light irradiation. The effects of Co_3O_4 on the light absorption, charge transfer process and photocatalytic activity were investigated systematically, and the photocatalytic mechanism was also explored. The novel Co_3O_4-g-C_3N_4 hetero-structured photocatalysts may have potential applications in environmental purifications.

2. Experimental

2.1. Synthesis of the photocatalysts

All chemicals were reagent grade and used without further purification. The metal-free g-C_3N_4 powders were synthesized by heating melamine in a muffle furnace. In a typical synthesis run, 5 g of melamine was placed in a semi-closed alumina crucible with a cover. The crucible was heated to 520 °C at a heating rate of 4 °C min^{-1}. Further deammoniation treatment was performed at 520 °C for 3 h. After the reaction, the alumina crucible was cooled to room temperature. The products were collected and ground into powders.

The preparation of Co_3O_4-g-C_3N_4 composite photocatalysts is described as follows: the as prepared g-C_3N_4 sample were added to 5 mL of distilled water containing an appropriate amount of $Co(NO_3)_2$ in a ceramic dish. The suspension was stirred using a glass rod during evaporation of water under the irradiation of an infrared light. The resulting powder was collected and calcined in air at 300 °C for 1 h in a muffle furnace. Then, Co_3O_4-g-C_3N_4 composite photocatalysts with different amounts of Co_3O_4 were obtained. The weight percentages of Co_3O_4 in the initial photocatalyst precursors were 0 wt%, 0.1 wt%, 0.2 wt%, 0.5 wt%, 0.8 wt%, 1.0 wt%, 1.5 wt% and 2.0 wt%, respectively.

2.2. Characterization

The crystal structure of samples was investigated using X-ray diffraction (XRD; Rigaka D/max 2500v/pc X-ray diffractometer) with Cu*K*α radiation at a scan rate of 4 min^{-1}. The accelerating voltage and the applied current were 40 kV and 40 mA, respectively. The morphology of the samples was examined by field emission scanning electron microscopy (SEM; FEI Quanta 200F; accelerating voltage = 10 kV) and transmission electron microscopy (TEM; JEOLJEM-2100; accelerating voltage = 200 kV). High-resolution transmission electron microscopy (HR-TEM, FEI Tecnai G2 F20) was operated at 200 kV to observe the crystallinity and arrangement of Co_3O_4-g-C_3N_4. UV–vis diffuse reflection spectroscopy (DRS) was performed on a Shimadzu UV-3100 spectrophotometer using $BaSO_4$ as the reference. The electron spin resonance (ESR) signals of spin-trapped oxidative radicals were obtained on a Bruker model ESR JES-FA200 spectrometer equipped with a quanta-Ray Nd:YAG laser system as the light source (λ=365/420 nm). The PL spectra of the photocatalysts were detected using a Varian Cary Eclipse spectrometer.

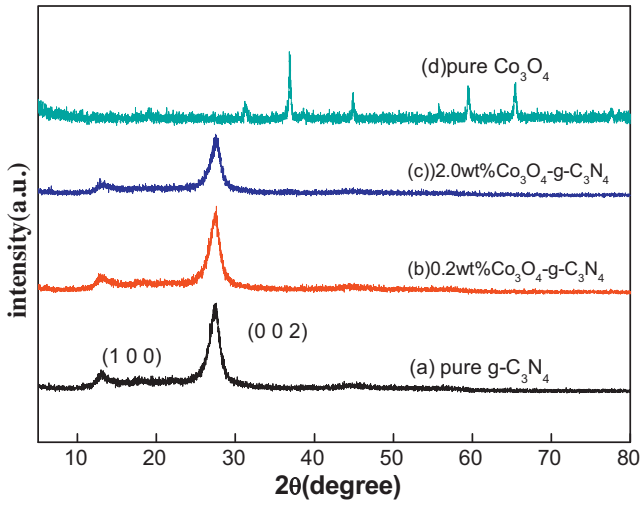

Fig. 1. XRD patterns of pure g-C_3N_4 and Co_3O_4, as well as of the Co_3O_4-g-C_3N_4 composite photocatalysts.

2.3. Photocatalytic activity

The photocatalytic activities of the Co_3O_4-g-C_3N_4 composite samples were evaluated via the photocatalytic degradation of methyl orange (MO) in aqueous solution under visible light irradiation. A 250 W Xe lamp with a 420 nm cutoff filter provided visible light irradiation. In each experiment, 0.1 g of photocatalyst was mixed with a 100 mL MO solution (10 mg L^{-1}). Prior to irradiation, the suspensions were magnetically stirred in the dark for 30 min to achieve a saturated MO absorption onto the catalyst. The irradiation time intervals of 1 h, the suspensions were collected and centrifuged (5000 rpm, 5 min) to remove the photocatalyst particles. The MO concentrations were monitored at 505 nm during the photodegradation process using a UV–vis spectrophotometer (Japan Shimadzu UV–vis1700).

3. Results and discussion

3.1. Characterization of Co_3O_4-g-C_3N_4 heterojunction samples

The powder XRD patterns of the as-prepared Co_3O_4-g-C_3N_4 samples are shown in Fig. 1. The results showed that the photocatalysts are crystalline. The XRD peaks of the pure g-C_3N_4 samples are in good agreement with the hexagonal phase of g-C_3N_4 (JCPDS 87-1526). The pure g-C_3N_4 sample shows two distinct peaks at 27.4° and 13.1°, which can be indexed as (0 0 2) and (1 0 0) diffraction planes. For the Co_3O_4-g-C_3N_4 composites, only g-C_3N_4 diffraction peaks are found when the Co_3O_4 content is below 2 wt%, which indicates that the doping of Co_3O_4 species does not affect the crystal structure of g-C_3N_4 photocatalysts. However, the diffraction intensities of the peak at 27.4° become weaker with increasing Co_3O_4 contents, which indicate that Co_3O_4 species restrain the growth of crystal structure of g-C_3N_4. No diffraction peaks of Co_3O_4 species are detected, which may be explained by the small amounts of

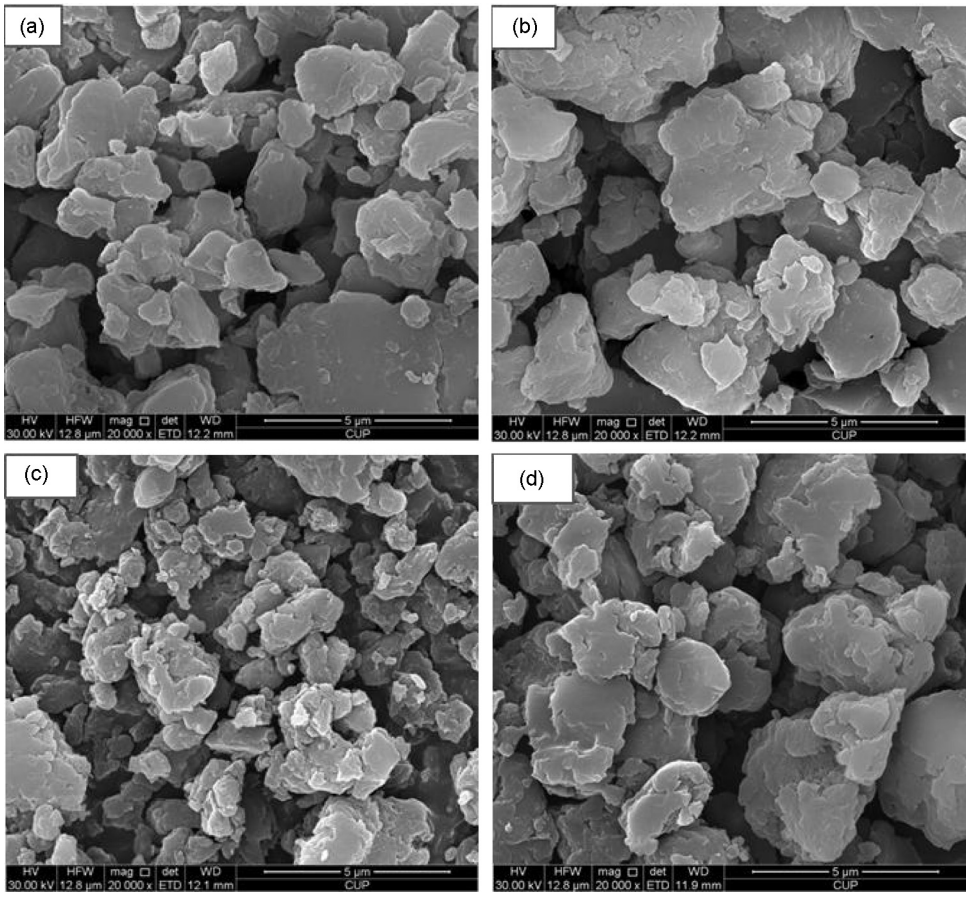

Fig. 2. SEM images of the Co_3O_4-g-C_3N_4 heterojunction photocatalysts: (a) pure g-C_3N_4; (b) 0.2 wt% Co_3O_4; (c) 1.0 wt% Co_3O_4; (d) 2.0 wt% Co_3O_4.

Co_3O_4 species introducing (maximal 2.0 wt%) and good dispersion in the composites.

The morphology and microstructure of the Co_3O_4-g-C_3N_4 heterojunction samples were characterized by SEM, TEM, and HRTEM. Fig. 2 shows the SEM micrographs of the as-prepared samples with different Co_3O_4 doping amount. The products exhibit aggregated particles, which contain many smaller crystals. After introducing Co_3O_4, the Co_3O_4-g-C_3N_4 heterojunction samples show agglomeration structures, which are similar to pure g-C_3N_4. The EDS of sample was performed to analyze the Co_3O_4 contents in the composite samples. The results indicate that the actual Co_3O_4 doping ratios are 0 wt%, 0.46 wt%, 1.39 wt%, 2.84 wt%, respectively, for the Co_3O_4-g-C_3N_4 samples designed with Co_3O_4 doping level at 0 wt%, 0.2 wt%, 1.0 wt%, 2.0 wt%. The morphology of the 0.2 wt% Co_3O_4-g-C_3N_4 composite was explored by TEM and HRTEM, showed in Fig. 3. The Co_3O_4-g-C_3N_4 sample mainly consists of 10–20 nm primary particles.

Fig. 4 presents the survey scan X-ray photoelectron spectroscopy (XPS) spectrum of the heterojunction sample. The binding energies obtained in the XPS analysis were corrected for specimen charging by referencing C 1s to 284.60 eV. It was carried out to determine the chemical states of the 0.2 wt% Co_3O_4-g-C_3N_4 samples and the valence states of various species present therein. The results indicated the presence of (b) C, (c) N, (d) Co, and (e) O, which may be due to the surface absorption and oxidation. Therefore, it may be concluded that the as-prepared samples is Co_3O_4-g-C_3N_4 phase. Fig. 4b shows the high-resolution XPS spectra of C 1s. Two peaks can be distinguished at 284.6 eV and 288.6 eV [37]. The major peak at 288.6 eV is exclusively assigned to carbon atoms (C–C bonding) in a pure carbon environment, i.e., graphitic or amorphous carbons either in our sample or adsorbed to the surface. The peak at 288.6 eV originates from carbon atoms bonded with three N neighbors in its chemical bone structure [38]. Fig. 4c presents the XPS spectrum of N 1s. The peak at 398.55 eV corresponds to N atoms [38]. The XPS data gives an evidence for the existence of graphite-like sp^2-bonded structure in graphitic carbon nitride. Fig. 4e shows the Co 2p XPS spectrum of the composite, which exhibits two peaks at 796.1 eV and 780.9 eV, corresponding to the Co $2p_{1/2}$ and Co $2p_{3/2}$ spin orbit. The presence of Co_3O_4 can be further confirmed by the O 1s XPS peak at 531.85 eV, which corresponds to the lattice oxygen in the Co_3O_4 phase. This result confirms the presence of Co_3O_4 in the g-C_3N_4 photocatalysts.

Optical absorption of the as-prepared pure g-C_3N_4 and Co_3O_4-g-C_3N_4 heterojunction samples was investigated using UV–vis spectrometer. As shown in Fig. 5, the g-C_3N_4 sample has photoabsorption from UV light to visible light, and the wavelength of the absorption edge is 460 nm, which could be responsible for the visible-light induced photocatalytic activity. After Co_3O_4 species was loaded, the absorption intensity in the visible light region was significantly improved, and the absorption commenced to enhance along with the increase of Co_3O_4 species content, corresponding colors shifted from yellowish to light grey. Based on the results of DRS, ESR and photocatalytic activity, the phenomenon may be attributed to a charge-transfer between the Co_3O_4 species and the g-C_3N_4. The wavelength threshold is determined by elongating the baseline and the steepest tangent of the UV–vis spectra and the wavelength of the intersection was λ_g. The wavelength threshold of the pure g-C_3N_4 samples is 463 nm, corresponding to the band gaps from 2.67 eV. After introducing Co_3O_4 co-catalyst, the visible light absorption of the composite samples is strengthened

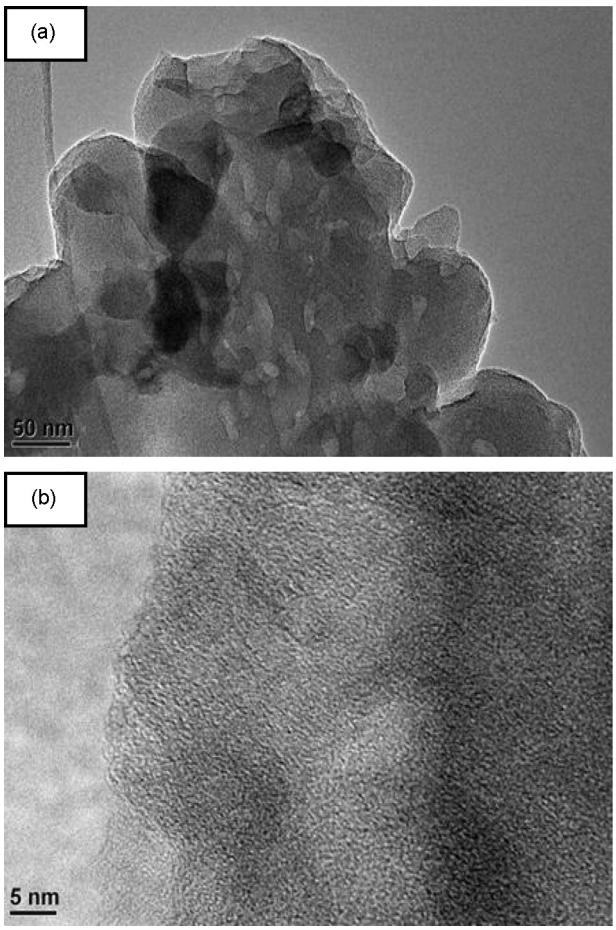

Fig. 3. TEM and HR-TEM images of the sample. (a) TEM micrographs of 0.2 wt% Co_3O_4-g-C_3N_4; (b) HR-TEM images of 0.2 wt% Co_3O_4-g-C_3N_4.

with increasing Co_3O_4 contents. The UV–vis results (Fig. 5) suggest that the composite samples may be able to absorb more visible light to produce electron–hole pairs and improve catalytic activity. Therefore, the visible light responses of these Co_3O_4-g-C_3N_4 composite samples are improved by the Co_3O_4 doping, and thus it may contribute to the enhancement of photoactivity of g-C_3N_4 samples.

3.2. Photocatalytic activity of the samples

The photocatalytic activities of as-prepared samples were evaluated by the degradation of organic dyes under visible light irradiation. Methyl orange (MO) was chosen as a representative hazardous dye to evaluate the photocatalytic performance, which showed a major absorption band at 505 nm. The photodegradation process of MO was recorded by the temporal evolution of the spectrum and all of the samples processed in the same procedure. Fig. 6 shows the photocatalytic activities of the Co_3O_4-g-C_3N_4 composite samples with different Co_3O_4 contents as well as pure g-C_3N_4 under visible light irradiation (λ>420 nm). The blank test confirms that methyl orange is only slightly degraded in the absence of catalysts, indicating that the photolysis can be ignored. Methyl orange degrades very slowly in the presence of pure g-C_3N_4 under visible light. Only 40% MO is photodegraded after irradiated for 3 h. However, the photocatalytic performance is significantly enhanced after modification by Co_3O_4, which indicates that the cobalt oxides play an important role in the enhancement of methyl orange degradation. Among them, the 0.2 wt% Co_3O_4-g-C_3N_4 photocatalyst exhibits the highest activity; methyl orange can be completely photodegraded under this condition. As shown in inset Fig. 6, the absorbance of methyl orange obviously decreases with increase of irradiation time. No absorbance peak is observed after irradiated for 3 h, which indicates complete methyl orange decomposition.

Photocatalytic results demonstrate that doping amount of Co_3O_4 has a great influence on the photocatalytic activity. As shown in Fig. 6, the degradation rate is 0.451, 0.529, 0.99, 0.864, 0.696, 0.638, 0.429, 0.235, respectively, for Co_3O_4-g-C_3N_4 0 wt%, 0.1 wt%, 0.2 wt%, 0.5 wt%, 0.8 wt%, 1.0 wt%, 1.5 wt%, 2.0 wt%. Thus, the optimal doping of Co_3O_4 on g-C_3N_4 is approximately 0.2 wt% from the experimental results and the photocatalytic activity is decreased with higher Co_3O_4 content. This can be attributed to the possibility that the excess Co_3O_4 species may act as recombination centers, and cover the active sites on the g-C_3N_4 surface and thereby reduce the efficiency of charge separation. Therefore, it is important to achieve a balance between the active trapping sites, which favoring the inhibition of the recombination of electron–hole pairs, and fewer trapped parts, which leading to a lower capacity for the separation of interfacial charge transfer. Based on our results, the photocatalytic activity of g-C_3N_4 modified by Co_3O_4 is effectively enhanced compared with that of pure g-C_3N_4 sample. The reason should be ascribed to the interaction between g-C_3N_4 and Co_3O_4, which takes an important role in the enhancement of photocatalytic performance. The 0.2 wt% Co_3O_4-g-C_3N_4 exhibited the highest photodegrading efficiency, which about 7.5-folds higher than that of pure g-C_3N_4. Co_3O_4 doping level is crucial to achieve the high photocatalytic activity of the Co_3O_4-g-C_3N_4 composite. The suitable Co_3O_4 doping can form a good dispersion on the g-C_3N_4 surface, which favored the separation and transfer of the charge carriers. However, a further increase of Co_3O_4 than 0.2 wt%, the photocatalytic activity was lowered. The introduction of a large of black Co_3O_4 can lead to shielding of the active sites on the photocatalyst surface, and also decrease the intensity of light through the depth of the reaction solution. As a consequence, a suitable content of Co_3O_4 is crucial for optimizing the photocatalytic performance of Co_3O_4-g-C_3N_4 composites. Therefore, the 0.2 wt% Co_3O_4-g-C_3N_4 is the best performing sample and was selected in the cycling study.

The stability of photocatalysts is important for its assessment and application. The cycling runs for the photo-oxidation of MO using the 0.2 wt% Co_3O_4-g-C_3N_4 photocatalysts were performed to evaluate its stability. The samples were washed with deionized water and dried after each cycling experiment. Fig. 7 shows the photodegradation of MO in every cycling runs, and there was slight catalyst deactivation in the fifth run. The reason can be ascribed to the slight loss of photocatalyst during the cycling runs. Along with cycling experiments (such as: washing, centrifugal and drying), the sample loss can be observed. After 5 runs of experiments, less photocatalyst was used in the photodegradation, leading to decrease of photocatalytic activity. Therefore, the deactivation of Co_3O_4-g-C_3N_4 is observed in fourth and fifth cycling run. Variations in the XRD analysis (Fig. 8) also illustrated that the crystal structure of the Co_3O_4-g-C_3N_4 photocatalysts did not change after the photocatalytic reaction. Therefore, the Co_3O_4-g-C_3N_4 composite can be regarded as stable photocatalysts in the experiments.

3.3. Photocatalytic mechanism discussion

To verify the photocatalytic mechanism, the ESR and PL techniques were performed. It is generally accepted that organic pollutants can be degraded by photocatalytic oxidation processes, in which a series of photo-induced reactive species, such as h^+, hydroxyl ($^\bullet OH$), superoxide ($^\bullet O_2^-$), are suspected to be involved in the photocatalytic degradation reaction. To elucidate the main reactive species responsible for the degradation of the organic contaminants over g-C_3N_4 photocatalyst, a series of quenchers

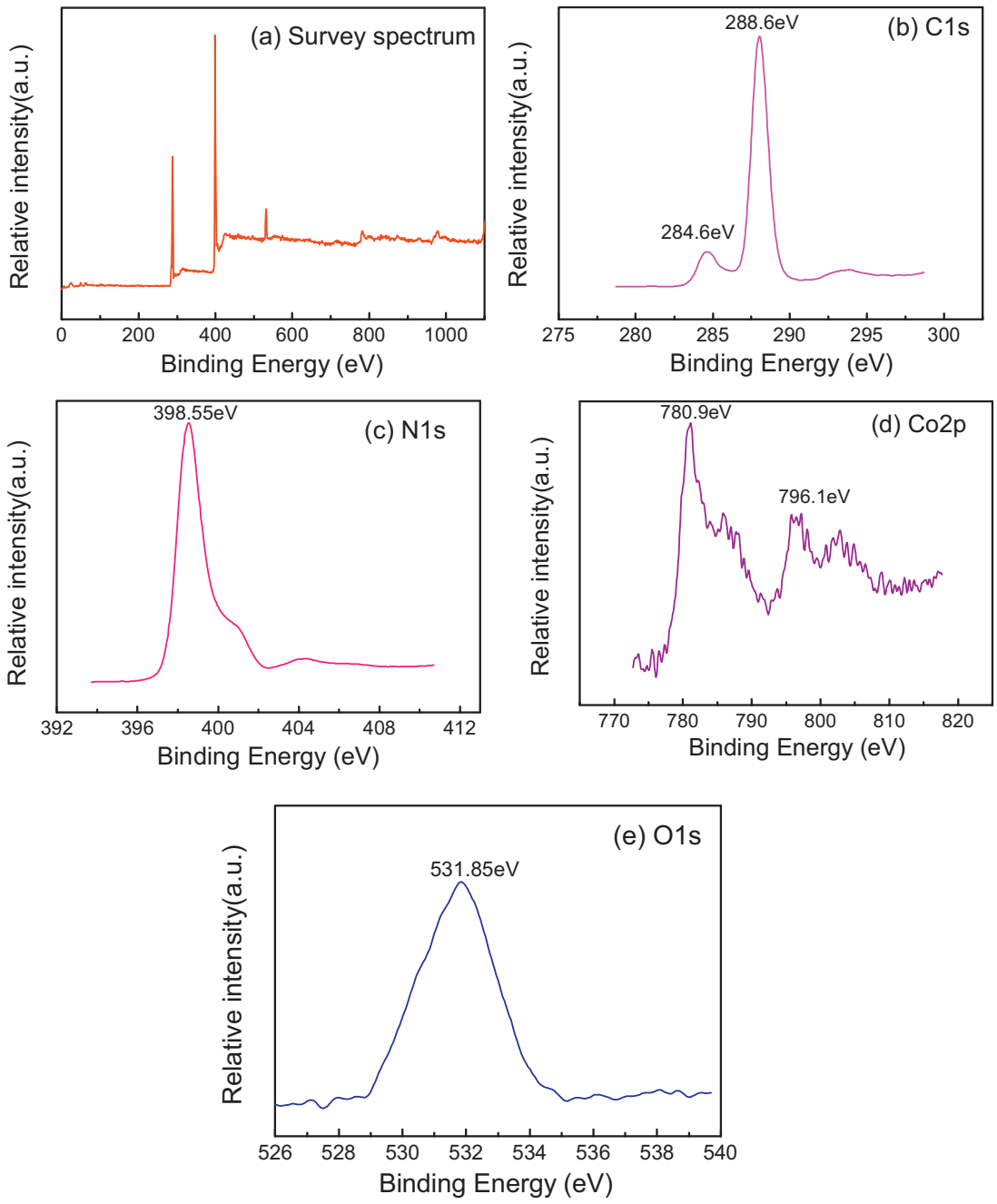

Fig. 4. XPS spectrum of the as-prepared 0.2 wt% Co_3O_4-g-C_3N_4 composite photocatalysts: (a)survey spectrum; (b) C 1s; (c) N 1s; (d) Co 2p; (e) O 1s.

were employed to scavenge the relevant reactive species. The ESR technique can be used to detect radicals in reaction systems [40]. Typically, DMPO (5,5-dimethyl-1-dimethyl *N*-oxide) generally used as a radical scavenger due to the generation of stable free radical, DMPO-$^{\bullet}O_2^-$ or DMPO-$^{\bullet}OH^-$.

Fig. 9 shows ESR spectra measured as the effect of light irradiation on the pure g-C_3N_4 and 0.2 wt% Co_3O_4-g-C_3N_4 photocatalyst at room temperature in air. Under visible light irradiation, significant evolution of ESR signals in H_2O and DMSO can be observed. As a comparison, no ESR signal was observed in the dark under otherwise identical conditions. Zhu et al. [41] reported a similar ESR results that only superoxide radical was produced by the photoactivated g-C_3N_4 nanorods under visible light irradiation. In this study, the intensity of radical signal for 0.2 wt% Co_3O_4-g-C_3N_4 is obviously stronger than g-C_3N_4 (Fig. 9 a–d), which indicates that the concentration of superoxide radicals ($^{\bullet}O_2^-$) in Co_3O_4-g-C_3N_4 sample is higher than that of pure g-C_3N_4. The result accounts for a higher photocatalytic activity of Co_3O_4-g-C_3N_4 than g-C_3N_4 toward the degradation of methyl orange. Furthermore, the signal of carbon free radicals was also found in pure g-C_3N_4 and 0.2 wt% Co_3O_4-g-C_3N_4 suspension in the presence of H_2O and DMSO. The carbon free radical derives from the structure of CN networks in g-C_3N_4 [41], which can stabilize and increase the lifetime of superoxide radicals, although it has no activity for degradation of organics. Therefore, compared with pure g-C_3N_4, the enhanced photocatalytic activity of 0.2 wt% Co_3O_4-g-C_3N_4 is mainly due to the larger amount and longer lifetime of oxidative radicals ($^{\bullet}O_2^-$), which is enriched and prolonged by the more stable carbon free radicals.

Combined with ESR results in the Fig. 9, superoxide radicals are still the main oxidative species for Co_3O_4-g-C_3N_4 samples. Therefore, the efficient photocatalytic degradation of MO can smoothly proceed. To further investigate the effect of Co_3O_4 modification,

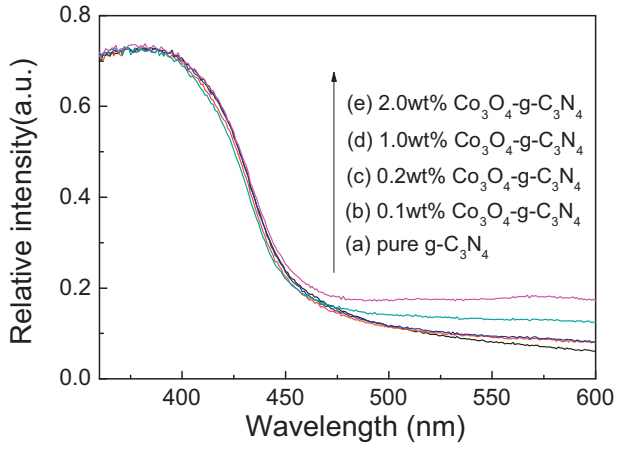

Fig. 5. UV–vis diffuse reflectance spectra of the as-prepared samples: (a) pure g-C_3N_4 (b) 0.1 wt% Co_3O_4-g-C_3N_4 (c) 0.2 wt% Co_3O_4-g-C_3N_4 (d) 1.0 wt% Co_3O_4-g-C_3N_4 (e) 2.0 wt% Co_3O_4-g-C_3N_4.

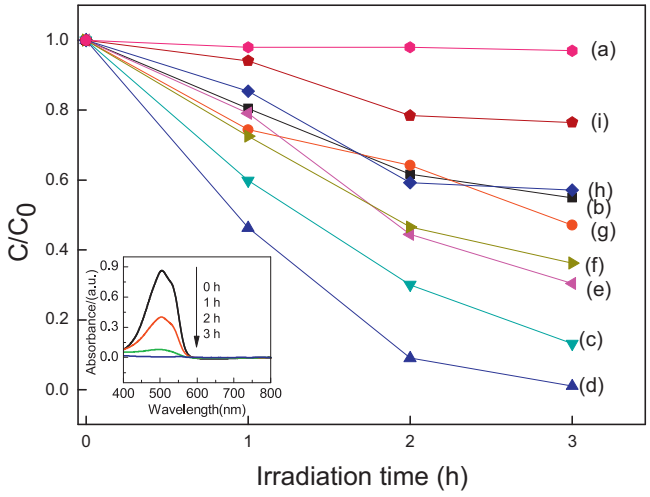

Fig. 6. Degradation rate of MO under visible light irradiation in the presence of Co_3O_4-g-C_3N_4 samples:(a) blank; (b) pure g-C_3N_4; (c) 0.1 wt% Co_3O_4-g-C_3N_4; (d) 0.2 wt% Co_3O_4-g-C_3N_4; (e) 0.5 wt% Co_3O_4-g-C_3N_4; (f) 0.8 wt% Co_3O_4-g-C_3N_4; (g) 1.0 wt% Co_3O_4-g-C_3N_4; (h) 1.5 wt% Co_3O_4-g-C_3N_4; (i) 2.0 wt% Co_3O_4-g-C_3N_4. The inset figure is the 0.2 wt% Co_3O_4-g-C_3N_4 samples degradation MO under light irradiation.

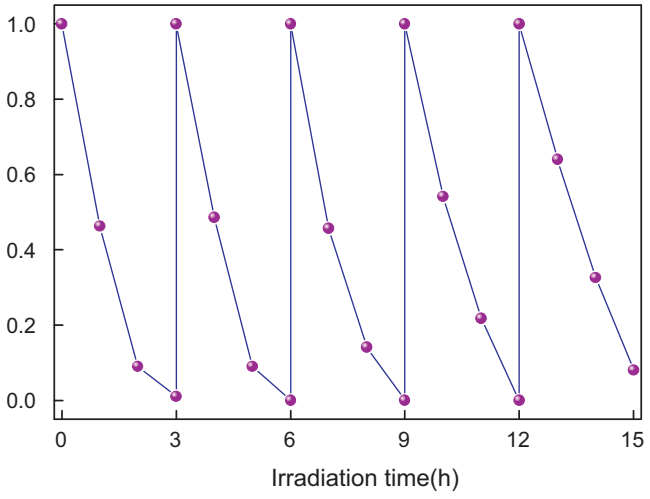

Fig. 7. Cycling runs for the photocatalytic MO in the presence of 0.2 wt% Co_3O_4-g-C_3N_4 composite under visible light irradiation.

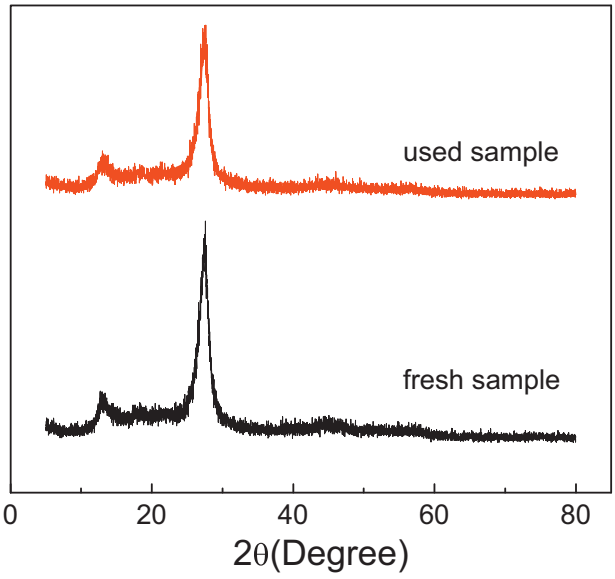

Fig. 8. XRD patterns of the 0.2 wt% Co_3O_4-g-C_3N_4 before and after the cycling photocatalytic experiments.

the PL spectra of Co_3O_4-g-C_3N_4 were performed. PL spectra reveal the migration, transfer, and recombination processes of the photo-generated electron–hole pairs in semiconductors. Fig. 10 presents the PL spectra of the Co_3O_4-g-C_3N_4 heterojunction sample and pure g-C_3N_4 photocatalysts at an excitation wavelength of 400 nm. At room temperature, the emission band for pure g-C_3N_4 was centered at 460 nm, which was attributed to the recombination process of self-trapped excitations. The positions of the Co_3O_4-g-C_3N_4 emission peaks were similar to g-C_3N_4. However, the emission intensity of the Co_3O_4-g-C_3N_4 composite photocatalysts significantly decreased, the 0.2 wt% Co_3O_4-g-C_3N_4 sample showed the weakest intensity. This result clearly indicated that the recombination of photo-generated charge carriers agreed well with the discussion on the charge carrier separation in photocatalytic experiments.

On the basis of the ESR and PL results, a possible mechanism for the MO photodegradation using the Co_3O_4-g-C_3N_4 heterojunction photocatalyst is proposed. The purpose is to guide the further improvement of the photocatalytic performance of the novel composite.

The metal-free g-C_3N_4 is a polymeric compound with graphitic planes constructed from tri-*s*-trizaine units, and connected by planar amino groups. The optical band gap of the polymer semiconductor is determined to be 2.7 eV. Therefore, g-C_3N_4 has the photocatalytic ability for water splitting and organic dye degradation under visible light irradiation. When Co_3O_4 was introduced into g-C_3N_4, the two types of semiconductor materials closely combined together and the heterojunction structure formed. The formation of Co_3O_4/g-C_3N_4 intimate interfaces is believed to promote the migration of photo-generated holes to the Co_3O_4 under visible light irradiation, leaving the electrons in the CB of g-C_3N_4, as shown in Fig. 11. Therefore, the recombination process of the electron–hole pairs was hindered, and charge separation as well as stabilization was achieved. The electrons in g-C_3N_4 photocatalysts are good reducing agents that could capture the adsorbed O_2 onto the composite catalyst surface and reduce it to $^{\bullet}O_2^-$ ($E^{\theta}(O_2/O_2^{\bullet-}) = -0.16$ V). And the holes transferred to cobalt oxides can also degrade the MO molecules. Therefore, we propose that the Co_3O_4-g-C_3N_4 heterojunction structure can enhance the separation of electron–hole pairs, and reduce the recombination of charge carriers, leading to the increase of the concentration of superoxide

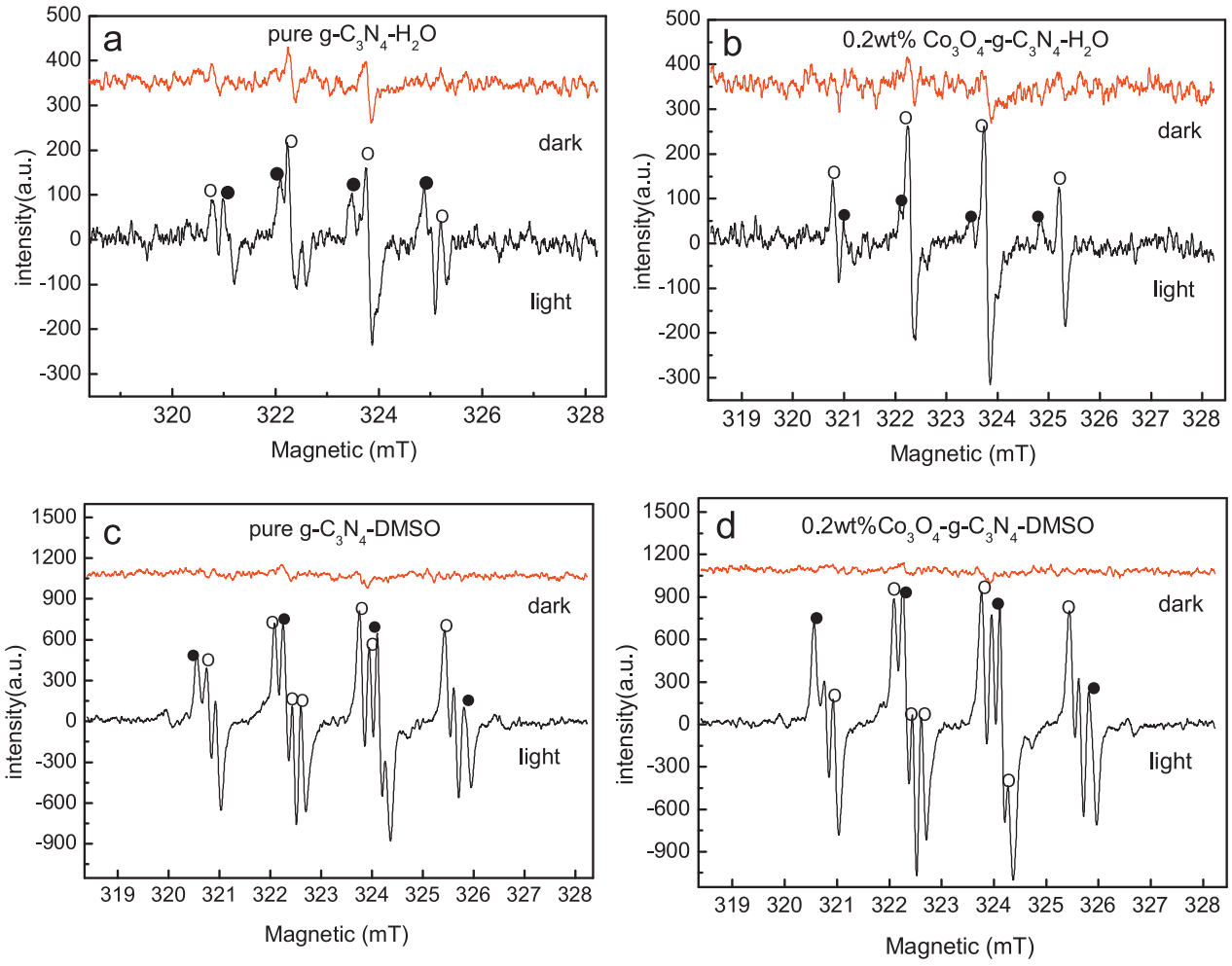

Fig. 9. ESR spectra of pure g-C_3N_4 and 0.2 wt% Co_3O_4-g-C_3N_4 photocatalysts in water and DMSO solvents ($\lambda > 420$ nm): (a) pure g-C_3N_4 in water; (b) 0.2 wt% Co_3O_4-g-C_3N_4 in water; (c) pure g-C_3N_4 in DMSO; (d) 0.2 wt% Co_3O_4-g-C_3N_4 in DMSO (DMPO as radical trapper, •label as carbon radicals, o label as superoxide radicals).

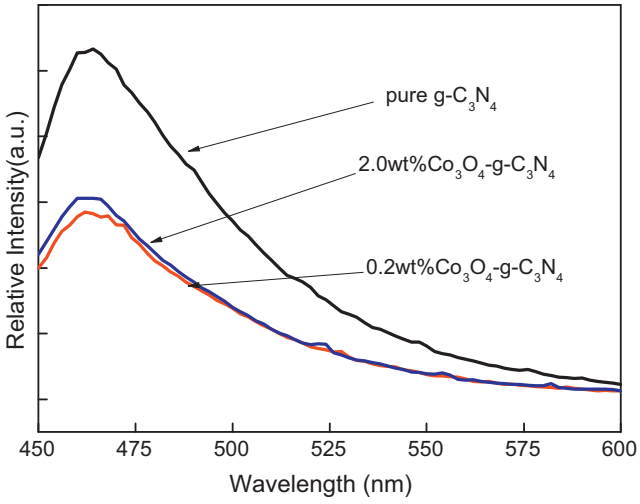

Fig. 10. Photoluminescence spectra (PL) of the Co_3O_4-g-C_3N_4 heterojunction photocatalysts.

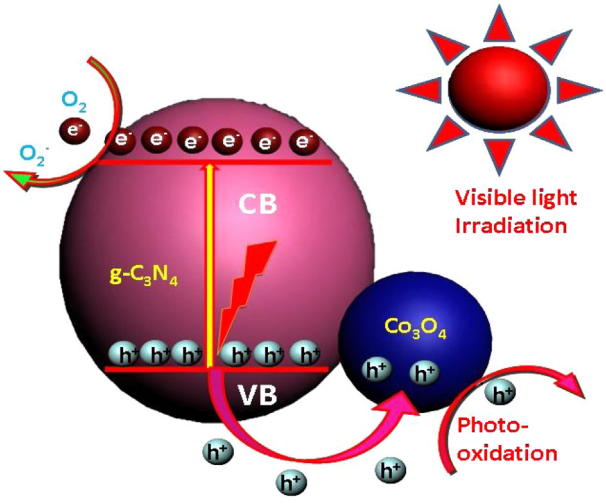

Fig. 11. The schematic diagram of methyl orange photodegradation over Co_3O_4-g-C_3N_4 heterojunction photocatalyst under visible light irradiation.

radicals ($^{\bullet}O_2^-$) involving in the photodegradation process. Thus, the cobalt oxides play an important role in improving photocatalytic performance.

4. Conclusions

Novel visible-light-induced Co_3O_4-g-C_3N_4 heterojunction photocatalysts were synthesized by introducing Co_3O_4 via a mixing-and-heating method. Cobalt species exists as Co_3O_4 and disperses on the surface of g-C_3N_4 to form the heterojunction structures. The doping of Co_3O_4 species did not affect the morphology and the crystal structure of g-C_3N_4 photocatalysts. The composite photocatalysts exhibited enhanced photocatalytic activity in the presence of small amounts of Co_3O_4 species, and the highest efficiency was observed with 0.2 wt% Co_3O_4-g-C_3N_4 sample, which is about a 7.5-fold enhancement than that of the pure g-C_3N_4. Superoxide radicals ($^{\bullet}O_2^-$) are the main oxidative species for Co_3O_4-g-C_3N_4 samples, and the presence of Co_3O_4 could increase the interfacial charge transfer and inhibit the recombination of electron–hole pairs, resulting in the increase of the number of main superoxide radicals in the photo-oxidation stage. A possible photocatalytic mechanism is proposed based on the experimental results. Therefore, the Co_3O_4-g-C_3N_4 is a promising photocatalytic material which can be potentially used for pollutants purification.

Acknowledgements

This work was financially supported by the National Science Foundation of China (Grant No. 21003157 and 21273285), Beijing Nova Program (Grant No. 2008B76), and Science Foundation of China University of Petroleum, Beijing (Grant No. KYJJ2012-06-20).

References

[1] X.F. Feng, S. Maier, M. Salmeron, J. Am. Chem. Soc. 134 (2012) 5662–5668.
[2] L. Ge, C.C. Han, X.L. Xiao, L.L. Guo, Int. J. Hydrogen Energy 38 (2013) 6960–6969.
[3] Y. Sun, G.X. Wang, K.P. Yan, J. Hazard. Mater. 36 (2011) 15502–15508.
[4] P. Adriana, L. Vincent, S. Kevin, G. Michael, T. Elijah, Nature 10 (2011) 456–461.
[5] L. Ge, J. Liu, Mater. Lett. 65 (2011) 1828–1831.
[6] Y.Q. Lan, C. Hu, X.X. Hu, A.M. Wang, Appl. Catal. B: Environ. 73 (2007) 354–360.
[7] L. Ge, C.C. Han, X.L. Xiao, L.L. Guo, Appl. Catal. B: Environ. 142–143 (2013) 414–422.
[8] C.D. Valentin, G. Pacchioni, A. Selloni, J. Phys. Chem. C 133 (2009) 20543–20552.
[9] S.K. Choi, S. Kim, S.K. Lim, H. Park, J. Phys. Chem. C 114 (2010) 16475–16480.
[10] R. Schaub, E. Wahlstrom, A. Ronnau, E. Lgsgaard, I. tensgaard, S.F. Besenbacher, Science 299 (2003) 377–379.
[11] J. Das, D. Khushalani, J. Phys. Chem. C 114 (2010) 8114.
[12] A. Kudo, Int. J. Hydrogen Energy 31 (2006) 197–202.
[13] G. Liu, P. Niu, C.H. Sun, S.C. Smith, Z.G. Chen, G.Q. Lu, H.M. Cheng, J. Am. Chem. Soc. 132 (2010) 11642–11648.
[14] R. Sasaki, K. Maeda, Y. Kako, K. Domen, Appl. Catal. B: Environ. 128 (2012) 72–76.
[15] S. Tokunaga, H. Kato, A. Kudo, Chem. Mater. 13 (2001) 4624–4628.
[16] F.F. Abdi, R.V.D. Krol, J. Phys. Chem. C 116 (2012) 9398–9404.
[17] W.J. Jo, J.W. Jang, K.J. Kong, H.J. Kang, J.Y. Kim, H. Jun, K.P.S. Parmar, J.S. Lee, Angew. Chem. Int. Ed. 51 (2012) 3147–3151.
[18] J.Z. Yang, J.W. Yu, J. Fan, D.P. Sun, W.H. Tang, X.J. Yang, J. Hazard. Mater. 189 (2011) 377–383.
[19] Z.J. Zhang, W.Z. Wang, M. Shang, W.Z. Yin, J. Hazard. Mater. 177 (2010) 1013–1018.
[20] X.H. Li, J.S. Zhang, X.F. Chen, A. Fischer, A. Thomas, M. Antonietti, X.C. Wang, Chem. Mater. 23 (2011) 4344–4348.
[21] L. Ge, F. Zuo, J.K. Liu, Q. Ma, C. Wang, D.Z. Sun, L. Bartels, P.Y. Feng, J. Phys. Chem. C 116 (2012) 13708–13714.
[22] J. Cao, B.D. Luo, H.L. Lin, S.F. Chen, J. Hazard. Mater. 190 (2011) 700–706.
[23] K. Nakashima, M. Kera, I. Fujii, S. Wada, Ceram. Int. 39 (2013) 3231–3234.
[24] X.C. Wang, K. Maeda, A. Thomas, K. Takamabe, G. Xin, J.M. Carlsson, K. Domen, M. Antonietti, Nat. Mater. 8 (2009) 76–80.
[25] S.C. Yan, Z.S. Li, Z.G. Zou, Langmuir 25 (2009) 10397–10401.
[26] S.C. Yan, Z.S. Li, Z.G. Zou, Langmuir 26 (2010) 3894–3901.
[27] S.C. Yan, S.B. Lv, Z.S. Li, Z.G. Zou, Dalton Trans. 39 (2010) 1488–1491.
[28] X.S. Zhou, B. Jin, L.D. Li, F. Peng, H.J. Wang, H. Yu, Y.P. Fang, J. Mater. Chem. 22 (2012) 17900–17905.
[29] L. Ge, C.C. Han, J. Liu, Y.F. Li, Appl. Catal. A: Gen. 409–410 (2011) 215–222.
[30] L. Ge, C.C. Han, J. Liu, Appl. Catal. B: Environ. 108–109 (2011) 100–107.
[31] L. Ge, C.C. Han, Appl. Catal. B: Environ. 117–118 (2012) 268–274.
[32] L. Ge, C.C. Han, J. Mater. Chem. 22 (2012) 11843–11850.
[33] F. Teng, M.D. Chen, N. Li, X. Hua, J. Wang, Q.Y. Zhang, Y. Wang, D.D. Meng, G.Q. Li, RSC Adv. 3 (2013) 743–751.
[34] Y.S. Luo, J.S. Luo, W.W. Zhou, X.Y. Qi, H. Zhang, D.Y.W. Yu, C.M. Li, H.J. Fan, T. Yu, J. Mater. Chem. A 1 (2013) 273–281.
[35] M. Kong, Y.Z. Li, X. Chen, T.T. Tian, P.F. Fang, F. Zhang, X.J. Zhao, J. Am. Chem. Soc. 133 (2011) 16414–16417.
[36] M. Long, W.M. Cai, J. Cai, B.X. Zhou, X.Y. Chai, Y.H. Wu, J. Phys. Chem. B 110 (2006) 20211–20216.
[37] X.W. Xie, Y. Li, Z.Q. Liu, M. Haruta, W.J. Shen, Nature 458 (2009) 746–749.
[38] X.H. Xia, J.P. Tu, Y.Q. Zhang, Y.J. Mai, X.L. Wang, C.D. Gu, X.B. Zhao, RSC Adv. 2 (2012) 1835–1841.
[39] J.S. Zhang, M. Grzelczak, Y.D. Hou, K. Maeda, K. Domen, X.Z. Fu, M. Antonietti, X.C. Wang, Chem. Sci. 3 (2012) 443–446.
[40] Y.J. Cui, Z.G. Ding, P. Liu, M. Antonietti, X.Z. Fu, X.C. Wang, Phys. Chem. Chem. Phys. 14 (2012) 1455–1462.
[41] X.J. Bai, L. Wang, R.L. Zong, Y.F. Zhu, J. Phys. Chem. C 117 (2013) 9952–9961.